Enhancing Performance of a GaAs/AlGaAs/GaAs Nanowire Photodetector Based on the Two-Dimensional Electron–Hole Tube Structure

Xiaotian Zhu, Fengyuan Lin, Zhihong Zhang, Xue Chen, Hao Huang, Dengkui Wang, Jilong Tang, Xuan Fang, Dan Fang, Johnny C. Ho, Lei Liao,* and Zhipeng Wei*

Read Online

ACCESS | Metrics & More | Article Recommendations | Supporting Information

ABSTRACT: Here, we design and engineer an axially asymmetric GaAs/AlGaAs/GaAs (G/A/G) nanowire (NW) photodetector that operates efficiently at room temperature. Based on the I-type band structure, the device can realize a two-dimensional electron–hole tube (2DEHT) structure for the substantial performance enhancement. The 2DEHT is observed to form at the interface on both sides of GaAs/AlGaAs barriers, which constructs effective pathways for both electron and hole transport in reducing the photocarrier recombination and enhancing the device photo-current. In particular, the G/A/G NW photodetector exhibits a responsivity of 0.57 A/W and a detectivity of 1.83×10^{10} Jones, which are about 7 times higher than those of the pure GaAs NW device. The recombination probability has also been significantly suppressed from 81.8% to 13.2% with the utilization of the 2DEHT structure. All of these can evidently demonstrate the importance of the appropriate band structure design to promote photocarrier generation, separation, and collection for high-performance optoelectronic devices.

KEYWORDS: GaAs, AlGaAs, nanowire, photodetector, two-dimensional electron–hole tube, photoresponse
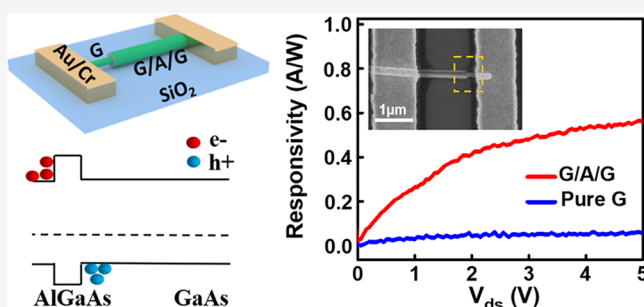
O wing to their unique dimensionality, finite-size effect, and superior surface-area-to-volume ratio, nanowires (NWs) have been demonstrated with great potentials as active materials for photoelectric devices, such as solar cells,[1,2] photodetectors,[3,4] lasers,[5,6] and light-emitting diodes.[7,8] Among these devices, photodetectors (PDs) fabricated by typical semiconductor NWs have become a research hotspot in recent years for their exceptionally high responsivity and detectivity.[4,9,10] In particular, gallium arsenide (GaAs) NWs are widely employed for the configuration of high-performance PDs because of its high electron mobility, appropriate direct band gap, and robust stability at room temperature;[11−13] however, there are still significant inherent material issues, including surface-related defects, to limit the obtained photocurrent, thus impeding the further improvement of responsivity.[3,14]

In general, the photocurrent of photodetectors is primarily governed by the generation, recombination, and transportation of photogenerated carriers. In this case, the photocurrent can be uplifted by three aspects. First, it is intuitive to create more photogenerated carriers in order to enhance the photocurrent. In other words, one can simply increase the population of photogenerated carriers, which participate in the photoelectric conversion processes, by utilizing narrow band gap semi-conductors as active PD materials[15,16] and/or constructing p–

n junctions accordingly.[17−19] Second, once the photogenerated carriers are excited, the corresponding carrier recombination is inevitable due to the presence of defects and trap states on the material surface. Therefore, it is effective to improve the photocurrent by suppressing the surface carrier recombination via different surface passivation schemes, such as preparing core−shell NW structures.[20,21] Finally, it is also beneficial to integrate the active semiconductor NWs with two-dimensional materials to enhance the carrier mobility such that the photogenerated carriers can be transported to the electrodes more efficiently for the improved photocurrent.[22−25] In semiconductor NWs, a two-dimensional electronic tube (2DET) can be established by accumulating a two-dimensional electron gas at the valence band edge of semiconductor heterojunctions.[3] This way, 2DET would be an advantageous device channel structure to substantially reduce the carrier recombination, while providing an effective pathway for
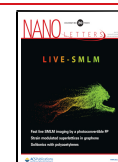
electron transport. Nevertheless, there are still certain limitations associated with these unidirectional tubes for the further device performance enhancement, especially for the case in p-type semiconductors in which the majority of carriers are dominated by holes.[26−30] In this regard, it would be ideal for constructing a structure containing both 2DET and two-dimensional hole tube (2DHT), where the effective electron and hole transport can then be achieved simultaneously in their respective channels with minimized carrier recombination. As a result, NW PDs configured with such device structure are anticipated to yield the record-high performance.

Here, we design and engineer a I-type device band structure for the enhanced NW PDs that can simultaneously realize both 2DET and 2DHT, namely, two-dimensional electron−hole tube (2DEHT) for simplicity, via the GaAs/AlGaAs/GaAs (G/A/G) axially asymmetric NW structure. The corresponding photoelectric device characteristics are analyzed thoroughly by measuring their current−voltage ($I-V$) curves, whereas the related PD properties can also be explicitly evaluated. It is impressive that, under 808 nm excitation, the fabricated PD with an axially asymmetric G/A/G NW structure can deliver a photocurrent of 2.24×10^{-12} A, a responsivity of 0.57 A/W, and a detectivity of 1.83×10^{10} Jones, where these responsivity and detectivity values are nearly 7 times higher than the ones of typical GaAs NW devices. In order to understand the transport and distribution of carriers in the 2DEHT structure, Silvaco Atlas is employed to perform the detailed theoretical analysis. Notably, 2DET and 2DHT are formed beside the two barriers of AlGaAs and GaAs, respectively, where they can promote the axial carrier transport and reduce the radial carrier diffusion, thereby suppressing the carrier recombination. As compared with the standard GaAs NW PDs, the axial asymmetry G/A/G NW structure here gives the higher photogenerated hole formation rate as well as the lower carrier recombination rate. The entire recombination probabilities are calculated to be 81.8% and 13.2%, respectively. All of these findings evidently indicate the potentials of adopting this 2DEHT structure for the substantial performance enhancement of NW photodetectors.

Results and Discussion. Figure 1a depicts the fabrication process of the photodetector based on a single axially asymmetric G/A/G NW, referring to "Methods" for the detailed process. Figure 1b shows the SEM image of a fabricated single G/A/G NW photodetector with the inset illustrating the enlargement of the heterojunction. It can be clearly observed that the diameter of the G/A/G NW in the unetched portion is not changed, while the diameter of the nanowire in the etched portion is significantly reduced to expose the core of the GaAs NW, suggesting the successful fabrication of this axially asymmetric G/A/G NW structure. At the same time, Figure 1c and Figure S2 sketch the energy band diagram of the 2DEHT structure designed in the G/A/G NW. It is noted that the I-type energy band structure formed on both sides of AlGaAs and GaAs. Since the intrinsic conduction and valence band offsets of GaAs/$Al_{0.4}Ga_{0.6}$As is 0.316 and 0.184 eV, respectively, the externally generated photoelectrons are blocked and aggregated by the barrier formed by the outer GaAs layer and AlGaAs. This way, a 2DET would be established at the outer AlGaAs/GaAs interface, inducing photogenerated electrons to propagate axially, suppressing the radial carrier diffusion. Meanwhile, the photogenerated holes produced by the internal GaAs layer are blocked by the AlGaAs barrier layer and would move to the metal electrode
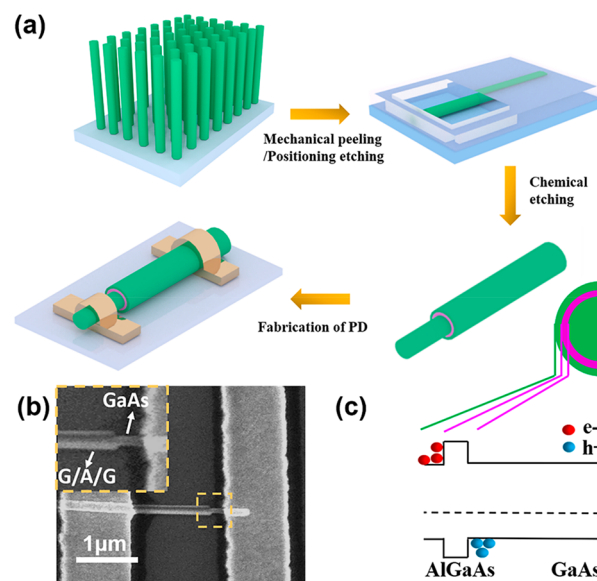
Figure 1. (a) Illustrative schematic of the fabrication process of a G/A/G NW photodetector. (b) SEM image of the fabricated single G/A/G NW photodetector with the inset showing the region of heterojunction. (c) Energy band diagram of the G/A/G NW channel along the radial direction.

under the electric field, forming a 2DHT at the inner AlGaAs/GaAs interface. These 2DET and 2DHT structures are anticipated to contribute the efficient carrier transport and collection for the realization of enhanced NW PDs, where the details will be discussed in the later sections.

The room-temperature photoresponse properties of both GaAs NW and G/A/G NW photodetectors are thoroughly investigated in terms of their output characteristics for different light intensities in Figure 2a,b. It is obvious that the
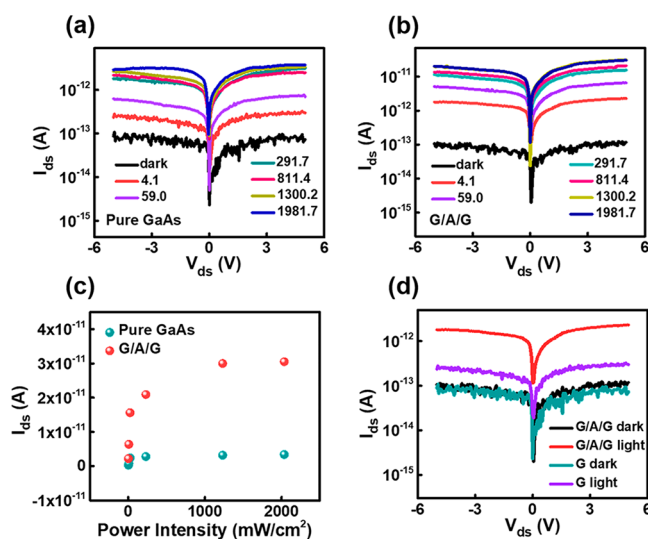
Figure 2. Output characteristics of photodetectors based on (a) a typical GaAs and (b) a G/A/G NW under dark and light illumination of 808 nm for different intensities. (c) Output current of both photodetectors as a function of illuminated light intensity at a drain bias of 5 V under the forward bias sweep measurement. (d) $I-V$ characteristics of both photodetectors under dark and light illumination (4.1 μW/cm^2). The gate bias is controlled at 0 V.

photocurrent increases with light illumination on account of the increased density of photogenerated carriers. The output characteristics of both dark and light currents under forward and reverse bias sweeps are asymmetric, which can be attributed to the different Schottky barrier results from the asymmetry of the NW device structure. By comparing the output characteristics of the pure GaAs NW photodetector and G/A/G NW photodetectors, it can be found that the photocurrent of the GaAs NW photodetector and G/A/G NW photodetector shows different trends under negative bias, where the G/A/G NW photodetector exhibits saturation under lower bias. The photogenerated carriers in G/A/G NW will transfer in the 2DEHT structure when excited, which greatly reduces the probability of collision between carriers and lattice defects, reduces the loss of carriers, and improves the collection of the device. As a result, the G/A/G NW can transmit more photogenerated carriers at a lower bias voltage, resulting in a higher photocurrent and earlier saturation. Figure 2c shows the dependence of the photocurrent on the light intensity of these two different devices at 5 V bias. At the same illumination power density, the photocurrent of the axially asymmetric G/A/G NW photodetector is an order of magnitude larger than the one of the pure GaAs NW photodetector, while the photocurrent of both devices increases with the increasing illumination power density. However, the increasing speed of the pure GaAs NW device slows down gradually, signifying the saturation of photocurrent. On the other hand, the G/A/G NW device does not exhibit this conspicuous carrier separation weakening at the high illumination power density. This phenomenon can be ascribed to the different carrier separation capabilities at varied illumination power densities. The built-in electric field near the Schottky junction of the pure GaAs NW device can separate photogenerated carriers more effectively at the lower illumination power density, while, at the higher power density, the built-in electric field would get weakened because the depletion region decreases with the increasing concentration of photogenerated carriers, weakening the carrier separation.[9,29,30] Figure 2d gives the $I-V$ characteristics of these two different devices under dark and light illumination of 808 nm at the gate voltage of 0 V. The dark currents of these devices do not have any significant difference, whereas, at an illumination power density of 4.1 μW/cm^2, the output current of the G/A/G NW photodetector can reach 2.24×10^{-12} A, which is 7 times higher than the one of the pure GaAs NW photodetector, indicating the enhanced carrier separation ability of the axially asymmetric NW structure.

Furthermore, Figure 3a,b demonstrates the dependence of responsivity (R) and detectivity (D^*) on the illumination power density of both G/A/G and pure GaAs NW photodetectors. When the incident light power density is 4.1 μW/cm^2 and the bias voltage is -5 V, the R and D^* of the photodetector fabricated from the axially asymmetric G/A/G NW with the 2DEHT structure are found to be 0.57 A/W and 1.83×10^{10} Jones, respectively, which are nearly 7 times higher than the ones (0.073 A/W and 2.69×10^9 Jones) of the pure GaAs NW device (see Calculations in Supporting Information). It is obvious that increasing the photocurrent is a crucial factor in improving device performance. It can be seen from Figure 2d that the I_{light} of the G/A/G NW photodetector with the 2DEHT structure is increased by 7 times as compared with that of the pure GaAs NW device, while the I_{dark} exhibits a negligible change such that the responsivity and detectivity of
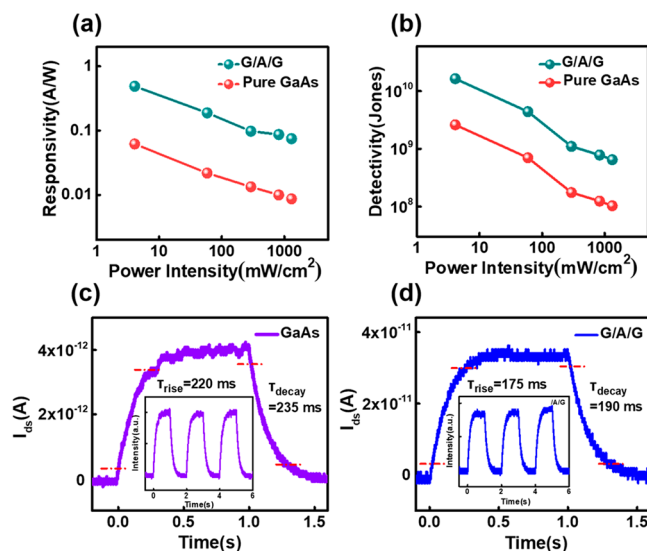
Figure 3. (a and b) Responsivity and detectivity of both GaAs and G/A/G NW photodetectors. (c and d) Transient response (device switching on and off) of both GaAs and G/A/G NW photodetectors achieved in one typical cycle. Insets show the responses of 3 complete cycles, indicating the repeatability.

the G/A/G device are significantly enhanced here. The origin of this performance enhancement of the G/A/G NW device can be explained due to the fact that the energy band offsets between GaAs and AlGaAs can enormously restrain the radial diffusion of carriers and then induce the electron and hole transport along the 2DET and 2DHT structures, respectively, in the horizontal direction. This way, the photogenerated carriers can be effectively separated with the minimized carrier recombination. As compared with the pure GaAs NW photodetector, bidirectional two-dimensional carrier tubes can facilitate the more efficient carrier transport and collection, thus generating a much larger photocurrent.[3] The switching response (device on- and off-states) of photodetectors can be evaluated by transient photoelectric current (TPC) measurements, as shown in Figure 3c,d. The response time is defined as the time interval from 10% to 90% (rise time) and from 90% to 10% (decay time) of the photocurrent signal.[22] In this work, the photodetectors are excited by a laser with a wavelength of 808 nm. The rise times of GaAs and G/A/G NW photodetectors are determined to be 220 and 175 ms, respectively, at 0 V bias. The corresponding decay times are found as 235 and 190 ms, accordingly, at 0 V bias. In principle, the rise time is determined by the carrier transport rate,[22] where this rate is heavily influenced by carrier scattering, chiefly collision between carriers and lattice defects. In our designed NW structure, 2DEHT can effectively restrain a large number of carriers in a small distance range, which significantly reduces the probability of carrier collision with lattice defects existing in the NW. Therefore, the rise time of the G/A/G NW device is substantially improved as compared with that of the pure GaAs NW photodetector. On the other hand, the decay time is mainly affected by the process of carrier recombination.[31] Since the 2DEHT structure of the G/A/G NW can efficiently separate the photogenerated carriers and reduce the carrier recombination, its decay time is also improved. At the same time, we provide the optical-electrical characteristics of the single unetched G/A/G NW photodetector under light illumination (808 nm) as shown in Figure S4. It is understood

that the realization of the 2DEHT NW structure would lead to performance enhancements in a broad prospect in photodetectors.

In order to fully understand the spatial distribution of photogenerated carriers in these NW photodetectors, the density distributions of carriers are simulated by the Silvaco Atlas simulation, as given in Figure 4. In the dark, the total
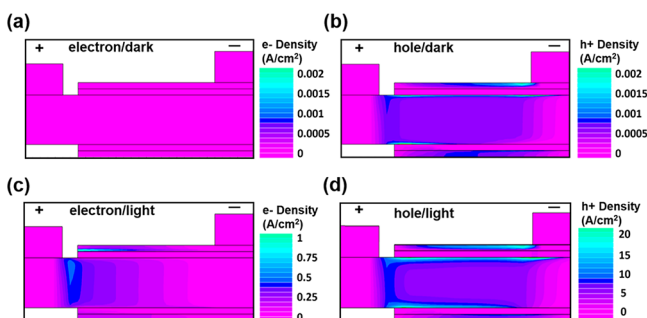
Figure 4. Two-dimensional profile of carrier distribution in G/A/G NW photodetectors. The simulated NW has a length of 4 μm and a diameter of 200 nm. (a and b) The electron current density and hole current density maps of photodetectors in the dark. (c and d) The electron current density and hole current density maps of a G/A/G NW photodetector under 808 nm excitation at -5 V bias.

current density in the photodetector is low, which is mainly due to the dominance of the hole current in the p-type NW, as shown in Figure 4a,b. In illumination conditions, photons are mainly absorbed by GaAs layers, owning to the narrow band gap, generating electron−hole pairs. Under the action of the externally applied voltage, the photogenerated electrons in the outer GaAs layer would move horizontally to the etching location and accumulate at the barrier between GaAs and AlGaAs. When the electric field provides enough energy, they can pass over the barrier and transfer to the inner GaAs layer. Eventually, they would be collected by the electrodes contacting the inner GaAs layer. Similarly, the holes would gather at the inner GaAs/AlGaAs interface and be transported in the 2DHT. When the electric field provided enough energy, they would cross over the barrier and be collected by the electrodes contacting the outer NW layer, as shown in Figure 4d. It can be clearly seen that there is almost no electron distribution in the location of the hole tube. Electrons are mainly transported along the GaAs core, as displayed in Figure 4c. In addition, simply calculating the product of the carrier generation rate and volume integral in Figure S7 can obtain the carrier population in different regions. It is concluded that in the core GaAs NW layer, the hole population in the 10 nm-wide 2DHT accounts for about 85.7% of the total carrier content there. Simultaneously, the carrier density distributions of the pure GaAs NW under dark and illuminated conditions is also simulated in Figure S6. It can be seen that both electron and hole concentrations of GaAs PD are almost the same in the radial direction. They gradually change in the axial direction with the maximum concentration near the electrodes. As compared with the pure GaAs NW PD under the same illumination power density, the designed G/A/G structure can successfully induce the spatial separation of electrons and holes, reduce the recombination of carriers, and increase the photocurrent, where all of these facts can be evidently witnessed in the I−V characteristics as presented in Figure 2. This device performance improvement comes definitely from

the remarkably enhanced photocurrent as introduced by the preeminent 2DEHT structure.

Through the analysis of band structure and carrier concentration distribution, it is also confirmed that the performance of the axially asymmetric G/A/G NW photodetector is much better than that of the pure GaAs NW photodetector because of the existence of 2DEHT. As compared with the pure GaAs NW photodetector, the axial asymmetric G/A/G NW photodetector has a higher photogenerated carrier concentration and the lower carrier recombination rate (see Calculations in Supporting Information), which proves again the advantageous role of the two-dimensional carrier tube. More importantly, the recombination probabilities can be assessed as 81.8% and 13.2% for pure GaAs NW and G/A/G NW PDs, accordingly, which indicate that the 2DEHT structure of the G/A/G NW can dramatically suppress the carrier recombination by establishing effective transport tubes for both electrons and holes. All of these effective carrier transport phenomena can also be confirmed by the simulation performed in Figure S7.

In conclusion, we have successfully fabricated enhanced photodetectors based on single axially asymmetric G/A/G NWs. The unique two-dimensional electron−hole tube (2DEHT) structures of G/A/G NWs are found to lead to the superior photoresponse of photodetectors. The responsivity of the G/A/G NW photodetector is evaluated to be 0.57 A/W, which is 7 times higher than that of pure GaAs NW photodetectors. Also, carrier transport simulations further illustrate that electrons and holes congregate on both sides of the barrier formed in the contact region between GaAs and AlGaAs, respectively. The electrons (holes) can then transport effectively along their electron (hole) tubes, which significantly reduces the recombination of carriers. All of these results can be thoroughly verified and confirmed by the I−V characteristics measured as well as the carrier recombination rate calculations. Importantly, this study not only demonstrates the potential of adopting a 2DEHT structure for enhanced photodetector performance but also evaluates the importance of the appropriate band structure design to promote photocarrier generation, separation, and collection for high-performance optoelectronic devices.

Methods. *NW Growth.* The GaAs/AlGaAs/GaAs NWs were synthesized on the undoped Si(111) substrate by a Ga-assisted self-catalyzed growth pattern in the DCA P600 MBE system. First, the GaAs core was synthesized on a substrate temperature of 600 °C, and then the V/III ratio was controlled = 25 and kept for 150 min. The GaAs cores are overgrown subsequently in situ by $Al_{0.4}Ga_{0.6}As$ and GaAs. The nominal thickness and Al content are obtained from the measured flux ratios and calibration values. The obtained NWs were eventually configured with a core−shell−shell structure consisting of a GaAs core (80 nm in radius), an AlGaAs shell (10 nm), and an outer GaAs shell (10 nm).

Photodetector Fabrication and Measurement. In this work, the single GaAs/AlGaAs/GaAs NW was successfully peeled off on a P^+ Si/SiO$_2$ (100 nm) substrate by mechanical peeling. Then, the uniform coating of methyl methacrylate (MMA) and poly(methyl methacrylate) (PMMA) was performed on the surface of the processed substrate. Next, electron beam lithography (EBL, JEOL 6510 with NPGS System) was carried out to achieve a window pattern on one end of the selected NW. This way, the exposed portion of the NW could be chemically etched by the prepared hydrogen

peroxide/citric acid etching solution for 5 s, followed by the removal of MMA and PMMA with deionized water. Finally, the Schottky-Ohmic contacted photodetectors would then be obtained using the metal electrode of Cr/Au (15 nm/50 nm). After device fabrication, the optoelectronic performance measurements of GaAs/AlGaAs/GaAs NW photodetectors were performed by an Agilent 4155C semiconductor parameter analyzer. The morphology of the prepared axially asymmetric G/A/G NW photodetector was characterized by a JSM-6510 scanning electron microscope.

■ ASSOCIATED CONTENT

ⓈⒾ Supporting Information

The Supporting Information is available free of charge at https://pubs.acs.org/doi/10.1021/acs.nanolett.0c00232.

SEM images, energy band diagram, external quantum efficiency of the photodetectors, output characteristics, two-dimensional profile, carrier concentration, and calculations (PDF)

■ AUTHOR INFORMATION

Corresponding Authors

Lei Liao — *State Key Laboratory for Chemo/Biosensing and Chemometrics, School of Physics and Electronics, Hunan University, Changsha 410082, China;* ⓞ orcid.org/0000-0003-1325-2410; Email: liaolei@whu.edu.cn

Zhipeng Wei — *State Key Laboratory of High Power Semiconductor Lasers, Changchun University of Science and Technology, Changchun 130022, China;* Email: zpweicust@126.com

Authors

Xiaotian Zhu — *State Key Laboratory of High Power Semiconductor Lasers, Changchun University of Science and Technology, Changchun 130022, China*

Fengyuan Lin — *State Key Laboratory of High Power Semiconductor Lasers, Changchun University of Science and Technology, Changchun 130022, China*

Zhihong Zhang — *State Key Laboratory of High Power Semiconductor Lasers, Changchun University of Science and Technology, Changchun 130022, China*

Xue Chen — *State Key Laboratory of High Power Semiconductor Lasers, Changchun University of Science and Technology, Changchun 130022, China;* ⓞ orcid.org/0000-0002-0413-1628

Hao Huang — *Department of Physics and Key Laboratory of Artificial Micro- and Nano-structures of Ministry of Education, Wuhan University, Wuhan 430072, China*

Dengkui Wang — *State Key Laboratory of High Power Semiconductor Lasers, Changchun University of Science and Technology, Changchun 130022, China*

Jilong Tang — *State Key Laboratory of High Power Semiconductor Lasers, Changchun University of Science and Technology, Changchun 130022, China*

Xuan Fang — *State Key Laboratory of High Power Semiconductor Lasers, Changchun University of Science and Technology, Changchun 130022, China;* ⓞ orcid.org/0000-0003-2290-4951

Dan Fang — *State Key Laboratory of High Power Semiconductor Lasers, Changchun University of Science and Technology, Changchun 130022, China*

Johnny C. Ho — *Department of Materials Science and Engineering, City University of Hong Kong, Hong Kong SAR 999077, China;* ⓞ orcid.org/0000-0003-3000-8794

Complete contact information is available at:
https://pubs.acs.org/10.1021/acs.nanolett.0c00232

Author Contributions

X.Z. and F.L. contributed equally to this work. L.L. and Z.W. conceived the project. X.Z. and H.H. performed device preparation. X.Z. and F.L. performed device characterization and wrote the manuscript together. Z.Z. and X.C. involved in device characterization. J.C.H. revised the entire manuscript. All authors analyzed and interpreted the data.

Notes

The authors declare no competing financial interest.

■ ACKNOWLEDGMENTS

■ REFERENCES

(1) Liu, R.; Wang, J.; Sun, T.; Wang, M.; Wu, C.; Zou, H.; Song, T.; Zhang, X.; Lee, S. T.; Wang, Z. L.; Sun, B. Silicon nanowire/polymer hybrid solar cell-supercapacitor: a self-charging power unit with a total efficiency of 10.5%. *Nano Lett.* **2017**, *17*, 4240−4247.

(2) Otnes, G.; Barrigon, E.; Sundvall, C.; Svensson, K. E.; Heurlin, M.; Siefer, G.; Samuelson, L.; Aberg, I.; Borgstrom, M. T. Understanding InP nanowire array solar cell performance by nanoprobe-enabled single nanowire measurements. *Nano Lett.* **2018**, *18*, 3038−3046.

(3) Dai, X.; Zhang, S.; Wang, Z.; Adamo, G.; Liu, H.; Huang, Y.; Couteau, C.; Soci, C. GaAs/AlGaAs nanowire photodetector. *Nano Lett.* **2014**, *14*, 2688−2693.

(4) Liu, X.; Gu, L.; Zhang, Q.; Wu, J.; Long, Y.; Fan, Z. All-printable band-edge modulated ZnO nanowire photodetectors with ultra-high detectivity. *Nat. Commun.* **2014**, *5*, 4007.

(5) Ho, J.; Tatebayashi, J.; Sergent, S.; Fong, C. F.; Iwamoto, S.; Arakawa, Y. Low-threshold near-infrared GaAs-AlGaAs core-shell nanowire plasmon laser. *ACS Photonics* **2015**, *2*, 165−171.

(6) Zhao, S.; Liu, X.; Woo, S. Y.; Kang, J.; Botton, G. A.; Mi, Z. An electrically injected AlGaN nanowire laser operating in the ultraviolet-C band. *Appl. Phys. Lett.* **2015**, *107*, 043101.

(7) Guo, W.; Zhang, M.; Banerjee, A.; Bhattacharya, P. Catalyst-free InGaN/GaN nanowire light emitting diodes grown on (001) silicon by molecular beam epitaxy. *Nano Lett.* **2010**, *10*, 3355−3359.

(8) Hayden, O.; Greytak, A. B.; Bell, D. C. Core-shell nanowire light-emitting diodes. *Adv. Mater.* **2005**, *17*, 701−704.

(9) Miao, J.; Hu, W.; Guo, N.; Lu, Z.; Zou, X.; Liao, L.; Shi, S.; Chen, P.; Fan, Z.; Ho, J. C.; Li, T.-X.; Chen, X. S.; Lu, W. Single InAs nanowire room-temperature near-infrared photodetectors. *ACS Nano* **2014**, *8*, 3628−3635.

(10) Butanovs, E.; Vlassov, S.; Kuzmin, A.; Piskunov, S.; Butikova, J.; Polyakov, B. Fast-Response Single-Nanowire Photodetector Based on ZnO/WS$_2$ Core/Shell Heterostructures. *ACS Appl. Mater. Interfaces* **2018**, *10*, 13869−13876.

(11) Wang, H. High gain single GaAs nanowire photodetector. *Appl. Phys. Lett.* **2013**, *103*, 093101.

(12) Luo, L. B.; Chen, J. J.; Wang, M. Z.; Hu, H.; Wu, C. Y.; Li, Q.; Wang, L.; Huang, J. A.; Liang, F. X. Near-Infrared Light Photovoltaic Detector Based on GaAs Nanocone Array/Monolayer Graphene Schottky Junction. *Adv. Funct. Mater.* **2014**, *24*, 2794−2800.

(13) Lu, Y.; Feng, S.; Wu, Z.; Gao, Y.; Yang, J.; Zhang, Y.; Hao, Z.; Li, J.; Li, E.; Chen, H.; Lin, S. Broadband surface plasmon resonance

enhanced self-powered graphene/GaAs photodetector with ultrahigh detectivity. *Nano Energy* **2018**, *47*, 140−149.

(14) Sun, M. H.; Joyce, H. J.; Gao, Q.; Tan, H. H.; Jagadish, C.; Ning, C. Z. Removal of surface states and recovery of band-edge emission in InAs nanowires through surface passivation. *Nano Lett.* **2012**, *12*, 3378−3384.

(15) Caroff, P.; Wagner, J. B.; Dick, K. A.; Nilsson, H. A.; Jeppsson, M.; Deppert, K.; Samuelson, L.; Wallenberg, L. R.; Wernersson, L. E. High-quality InAs/InSb nanowire heterostructures grown by metal-organic vapor-phase epitaxy. *Small* **2008**, *4*, 878−882.

(16) Svensson, J.; Anttu, N.; Vainorius, N.; Borg, B. M.; Wernersson, L. E. Diameter-dependent photocurrent in InAsSb nanowire infrared photodetectors. *Nano Lett.* **2013**, *13*, 1380−1385.

(17) Dao, T. D.; Dang, C. T. T.; Han, G.; Hoang, C. V.; Yi, W.; Narayanamurti, V.; Nagao, T. Chemically synthesized nanowire TiO$_2$/ZnO core-shell pn junction array for high sensitivity ultraviolet photodetector. *Appl. Phys. Lett.* **2013**, *103*, 193119.

(18) Ma, L.; Hu, W.; Zhang, Q.; Ren, P.; Zhuang, X.; Zhou, H.; Xu, J.; Li, H.; Shan, Z.; Wang, X.; Liao, L.; Xu, H. Q.; Pan, A. Room-temperature near-infrared photodetectors based on single hetero-junction nanowires. *Nano Lett.* **2014**, *14*, 694−698.

(19) Li, L.; Gu, L.; Lou, Z.; Fan, Z.; Shen, G. ZnO Quantum Dot Decorated Zn$_2$SnO$_4$ Nanowire Heterojunction Photodetectors with Drastic Performance Enhancement and Flexible Ultraviolet Image Sensors. *ACS Nano* **2017**, *11*, 4067−4076.

(20) Gao, L.; Zeng, K.; Guo, J.; Ge, C.; Du, J.; Zhao, Y.; Chen, C.; Deng, H.; He, Y.; Song, H.; Niu, G.; Tang, J. Passivated Single-Crystalline CH$_3$NH$_3$PbI$_3$ Nanowire Photodetector with High Detectivity and Polarization Sensitivity. *Nano Lett.* **2016**, *16*, 7446−7454.

(21) Jeong, S.; Choe, M.; Kang, J. W.; Kim, M. W.; Jung, W. G.; Leem, Y. C.; Chun, J.; Kim, B. J.; Park, S. J. High-performance photoconductivity and electrical transport of ZnO/ZnS core/shell nanowires for multifunctional nanodevice applications. *ACS Appl. Mater. Interfaces* **2014**, *6*, 6170−6176.

(22) Wu, Y.; Yan, X.; Zhang, X.; Ren, X. A monolayer graphene/GaAs nanowire array Schottky junction self-powered photodetector. *Appl. Phys. Lett.* **2016**, *109*, 183101.

(23) Li, X.; Lin, S.; Lin, X.; Xu, Z.; Wang, P.; Zhang, S.; Zhong, H.; Xu, W.; Wu, Z.; Fang, W. Graphene/h-BN/GaAs sandwich diode as solar cell and photodetector. *Opt. Express* **2016**, *24*, 134−145.

(24) Shao, D.; Yu, M.; Sun, H.; Hu, T.; Lian, J.; Sawyer, S. High responsivity, fast ultraviolet photodetector fabricated from ZnO nanoparticle-graphene core-shell structures. *Nanoscale* **2013**, *5*, 3664−3667.

(25) Clifford, J. P.; Konstantatos, G.; Johnston, K. W.; Hoogland, S.; Levina, L.; Sargent, E. H. Fast, sensitive and spectrally tuneable colloidal-quantum-dot photodetectors. *Nat. Nanotechnol.* **2009**, *4*, 40−44.

(26) Du, J.; Liu, Y.; Mo, J.; Zhao, Z.; Huang, S.; Liu, Y.; Yu, Q. Design and simulation of a nanoscale GaN-based vertical HFET with pnp-superjunction buffer structure. *Nanosci. Nanotechnol. Lett.* **2015**, *7*, 100−104.

(27) Zhao, Q. X.; Willander, M.; Bergman, J. P.; Holtz, P. O.; Lu, W.; Shen, S. C. Dynamic properties of radiative recombination in p-type δ-doped layers in GaAs. *Phys. Rev. B: Condens. Matter Mater. Phys.* **2001**, *63*, 125337.

(28) Sampath, A. V.; Zhou, Q. G.; Enck, R. W.; McIntosh, D.; Shen, H.; Campbell, J. C.; Wraback, M. P-type interface charge control layers for enabling GaN/SiC separate absorption and multiplication avalanche photodiodes. *Appl. Phys. Lett.* **2012**, *101*, 093506.

(29) Ali, H.; Zhang, Y.; Tang, J.; Peng, K.; Sun, S.; Sun, Y.; Song, F.; Falak, A.; Wu, S.; Qian, C.; Wang, M.; Zuo, Z.; Jin, K. J.; Sanchez, A. M.; Liu, H.; Xu, X. High-Responsivity Photodetection by a Self-Catalyzed Phase-Pure p-GaAs Nanowire. *Small* **2018**, *14*, No. 1704429.

(30) Hu, Y.; Chang, Y.; Fei, P.; Snyder, R. L.; Wang, Z. L. Designing the electric transport characteristics of ZnO micro/nanowire devices by coupling piezoelectric and photoexcitation effects. *ACS Nano* **2010**, *4*, 1234−1240.

(31) Chen, X.; Xia, N.; Yang, Z.; Gong, F.; Wei, Z.; Wang, D.; Tang, J.; Fang, X.; Fang, D.; Liao, L. Analysis of the influence and mechanism of sulfur passivation on the dark current of a single GaAs nanowire photodetector. *Nanotechnology* **2018**, *29*, 095201.